Available online at www.easd.procedia.org
EASD Procedia EURODYN (2026) 871-886

EASD Procedia

EURODYN 2026
XIII International Conference on Structural Dynamics
M. Beer, C. Papadimitriou, H. Jensen, J. Chen, M. Broggi, J. Behrensdorf (eds.)
Hannover, Germany, 27.09.–01.10 2026

DUAL-GYRO NONLINEAR CONTROL FOR ROLL-YAW ATTENUATION IN HIGH-SPEED CRAFTS

G. Pepe[1], M. Laurenza[2], A. Carcaterra[1], N. Roveri[1], L. Cortese[1] and A. Culla[1]

[1]Department of Mechanical and Aerospace Engineering, University of Rome La Sapienza
Via Eudossiana, 18, 00184 Rome, Italy
e-mail: {gianluca.pepe, antonio.carcaterra, nicola.roveri, luca.cortese, antonio.culla}@uniroma1.it

[2] Department of Engineering, Niccolò Cusano University
Via Don Carlo Gnocchi, 3, 00166 Rome, Italy
e-mail: maicol.laurenza@unicusano.it

Keywords: Dual gyrostabilizers, Nonlinear control, Passenger comfort, Roll–yaw attenuation.

Abstract. *We present a nonlinear control framework for roll and yaw attenuation in a high-speed passenger craft equipped with two gyrostabilizers. The vessel is modeled with a 6-DOF maneuvering formulation augmented by the gyroscope dynamics, explicitly coupling spin and precession torques with the hull, using hydrodynamic coefficients obtained from frequency-domain potential-flow analyses and hydrostatic contributions evaluated online during simulation. Three active control strategies based on the Feedback Local Optimality Principle (FLOP) are compared against an uncontrolled baseline and a passive configuration: a roll-oriented strategy, a comfort-oriented strategy targeting vertical accelerations weighted according to ISO 2631, and an asynchronous strategy exploiting differential precession to generate a net yaw moment, reducing rudder load while maintaining roll stabilization. Simulation results show that active FLOP control consistently outperforms the passive baseline across all tested conditions. The comfort-oriented strategy achieves targeted reductions in the motion sickness dose value when roll is the dominant source of vertical acceleration, but loses effectiveness when pitch becomes the primary contributor — a condition not controllable with the present two-gyroscope configuration. The asynchronous strategy demonstrates that differential precession is an effective means of redistributing control authority between roll stabilization and yaw management at marginal additional gyro cost. Results highlight the dependence of optimal strategy selection on sea state severity, wave heading, and target performance metric.*

ISSN:2311-9020 © 2026 The Authors. Published by EASD Procedia.
Peer-review under responsibility of the Organizing Committee of EURODYN 2026.
doi: 10.47964/1326.10704.205

1 INTRODUCTION

Roll motion mitigation represents a key issue in the dynamics and control of high-speed vessels, as it directly affects both operational safety and onboard comfort. Wave-induced motions can easily generate accelerations exceeding acceptable thresholds for human exposure, potentially leading, in severe and prolonged conditions, to adverse physiological effects [1]. For this reason, the active reduction of vessel motions plays a central role in both seakeeping performance and high-speed passenger transport.

Among the available solutions, internal gyroscopic stabilizers offer significant advantages over external hydrodynamic appendages, as their effectiveness does not depend on the forward speed of the vessel [2, 3]. In recent years, advances in materials and control technologies have renewed interest in these devices within the naval domain, with promising experimental and numerical results [4–6].

From a control perspective, a large portion of the naval literature has focused on linear, single-degree-of-freedom approaches targeting roll dynamics only, often neglecting the coupling with pitch and yaw [2, 7]. This reflects a simplified interpretation of gyroscopic actuation: while in the Control Moment Gyroscope (CMG) literature in aerospace and robotics the simultaneous generation of moments along multiple axes is a fundamental feature exploited for coordinated multi-axis control [8–10], in the naval field the additional moment components have typically been treated as undesirable side effects.

In particular, the yaw moment generated by gyroscopic action has traditionally been regarded as a disturbance to be minimized [3], rather than as a resource that can be actively exploited within the control design. Within this framework, even more advanced control strategies, such as Linear Quadratic Regulation (LQR), adaptive control, and Model Predictive Control (MPC), although effective in handling actuator constraints and improving roll attenuation [6, 11], are often based on linearized models or lead to significant computational burden when dealing with strong nonlinearities and competing objectives.

More fundamentally, a mismatch often arises between the control objectives and the performance metrics used for evaluation. In many studies, roll reduction is assumed not only as the primary control objective but also as a proxy for overall performance. However, this assumption is limited, particularly in passenger transport applications, where onboard comfort is strongly influenced by vertical accelerations and their spectral content, which are more directly related to human perception and vibration exposure [1]. In addition, the interaction between gyroscopic moments and yaw dynamics can affect the load required by the steering system, with implications for maneuverability and overall energy consumption. This motivates the need for control formulations in which the objective functions explicitly reflect comfort, operability, and energy efficiency, rather than focusing solely on roll attenuation.

In this work, a full six-degree-of-freedom model of the vessel, coupled with the dynamics of two internal gyroscopic stabilizers, is adopted, extending the nonlinear control framework previously developed in [12] to a multi-objective formulation that also accounts for yaw dynamics. The Feedback Local Optimality Principle (FLOP) is employed as the feedback control strategy. The proposed formulation allows the inclusion in the cost function of both roll stabilization objectives and comfort indicators compliant with ISO 2631, as well as nonlinear terms that exploit the operational limits of the gyroscopes without violating physical constraints. Furthermore, the gyroscopic effect on yaw is actively leveraged to reduce the load on the steering system, framing the stabilization problem as an integrated control task addressing stability, comfort, and energy efficiency of marine operations.

Within this perspective, the proposed approach differs from recent MPC- and adaptive-control strategies for gyrostabilizer-equipped vessels [6, 11], which have mainly focused on roll attenuation and actuator-constraint handling. Here, comfort and directional-control objectives are not evaluated only as secondary performance indicators, but are embedded directly in the feedback design through an algebraic, real-time-compatible control law. The approach also differs from CMG-based multi-axis control frameworks developed in aerospace and robotics [8–10], where multiple actuators are coordinated to achieve general torque allocation. In the present marine configuration, the two gyrostabilizers are instead used in a deliberately constrained way: asynchronous precession redistributes part of the available gyroscopic authority between roll attenuation and yaw-load reduction, without introducing additional actuators beyond those already required for roll stabilization. More broadly, this perspective is consistent with recent trends in marine systems research, where energy-aware operation plays a central role in guidance, coordination, and mission planning [13, 14].

2 INTEGRATED SHIP-GYROSTABILIZER SYSTEM

As a representative case study, the analysis considers a high-speed semi-displacement passenger catamaran belonging to a class of vessels widely employed in short- and medium-range transport services, where reduced travel times, high service frequency, and onboard comfort constitute key operational requirements. Vessels of this type are commonly used for fast connections along coastal routes and between mainland and island destinations, typically carrying several hundred passengers over relatively short distances at sustained cruising speeds. Their operational profile is generally characterized by intensive service over a significant portion of the year and under variable sea conditions, ranging from seasonally mild to more demanding environments. For these reasons, this class of craft provides a meaningful benchmark for assessing the effectiveness of advanced stabilization strategies under realistic operating conditions. The vessel is equipped with twin diesel waterjet propulsion, and its main geometric and inertial parameters are reported in Table 1. The twin-hull configuration also provides the internal volume required to integrate the gyrostabilization system without modifications to the hull geometry.

The stabilization system consists of two gyroscopic units operating in an asynchronous configuration, installed symmetrically within the two hulls in the vicinity of the longitudinal center of mass (Figure 1). This arrangement enables a balanced distribution of the additional onboard mass, limits variations in static trim, and reduces possible structural coupling effects between the devices. The main gyroscope parameters, obtained by sizing the stabilization system with reference to the commercial VEEM VG70 Mark II gyrostabilizer, are reported in Table 2.

The adoption of two units is motivated not only by installation and mass-balancing requirements, but also by a specific control choice. In conventional synchronous configurations commonly adopted in marine applications, the gyroscopes are operated so as to compensate, or at least significantly attenuate, the moment components generated about the yaw axis. Within this framework, such contributions are generally regarded as undesirable side effects, while the control action remains essentially focused on roll mitigation alone.

In the present work, a different strategy is deliberately pursued: the two devices are controlled independently, so that their combined action is not restricted to roll reduction only. As will be shown in the following sections, the proposed control formulation makes it possible to actively exploit the gyroscopic moment about the yaw axis as an additional control resource, thus contributing to the directional dynamics of the vessel and reducing the action demanded from the steering system, with a potential benefit also in terms of absorbed power. From this perspective, stabilization is addressed as an integrated problem, in which roll attenuation,

directional control, and reduction of steering effort are treated as coupled objectives, rather than as separate or competing effects.

Table 1: Main parameters of the reference catamaran.

Quantity	Value	Unit
Mass m	107×10^3	kg
Roll inertia I_{xx}	10×10^5	kg m^2
Pitch inertia I_{yy}	8×10^5	kg m^2
Yaw inertia I_{zz}	9×10^5	kg m^2
Transverse metacentric height GM_t	17	m
Longitudinal metacentric height GM_l	94.0	m
Length overall L_{OA}	35.0	m
Beam B	9.4	m
Draft T	0.8	m
Displacement Δ	9,400	kg

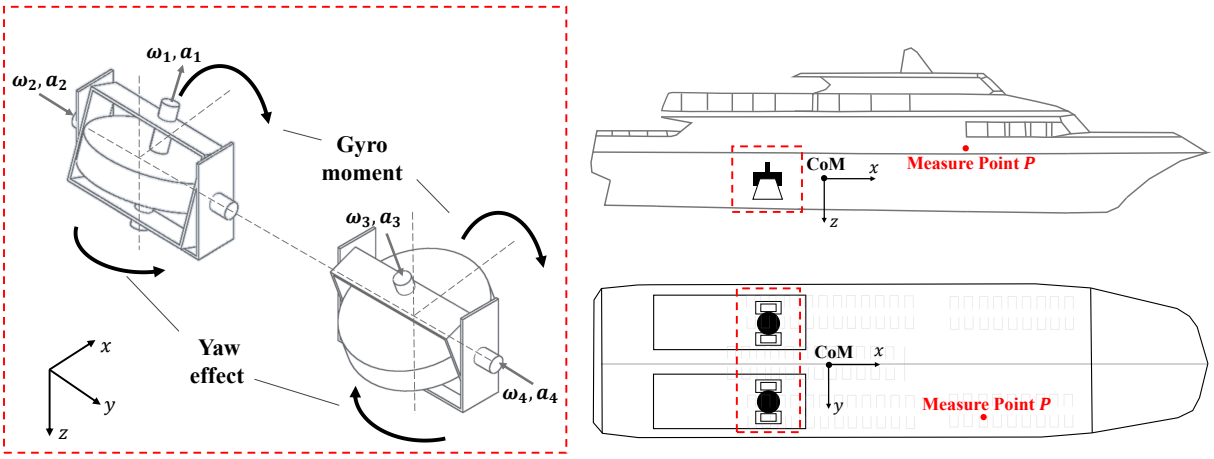


Figure 1: Layout of the gyroscopic stabilization system adopted for the catamaran. The left panel illustrates the gyroscopic units and the moments generated during operation, whereas the right panel shows their symmetric installation within the two hulls, along with the position of the vessel center of mass (CoM) and the measurement point used in the analysis.

2.1 Nonlinear vessel model

The model adopted in this work is a nonlinear, fully coupled representation of the reference ship–gyro system and is used as the main plant for the numerical investigations. The formulation builds upon the standard 6-DOF maneuvering framework for marine craft dynamics [15], which is here extended to account for the internal dynamics of two gyrostabilizers. In this way, hull motion, gyro actuation, and gyroscopic coupling are treated within a unified multibody framework. The resulting model is enriched by hydrostatic restoring effects, added mass, linear and nonlinear hydrodynamic damping, environmental disturbances due to waves and wind, and the gravitational contribution of the coupled mechanical system.

A further layer of complexity is introduced by the radiation-memory effects, which are represented through an auxiliary state-space subsystem. As a result, the overall model dimension

Table 2: Main parameters of the onboard gyrostabilizers VG70 Mark II.

Quantity	Value	Unit
Angular momentum	70	kN m s
Nominal torque	145	kN m
Mass	2850	kg
Maximum power	18	kW
Rotor speed	4800	rpm
Maximum precession speed $\omega_{\max}$	2	rad/s

exceeds that associated with the sole physical degrees of freedom, while retaining a time-domain formulation suitable for simulation and control analysis. This model thus plays a double role: it represents the reference vessel used for performance assessment, and it provides the dynamical backbone for the subsequent model-based control design. In practice, the controller is built on a control-oriented representation compatible with the state information that can realistically be measured or estimated, whereas the complete model is retained as the high-fidelity benchmark for closed-loop evaluation.

The vessel configuration is described by the position and attitude vector $\boldsymbol{\eta} = [x, y, z, \phi, \theta, \psi]^T$, expressed in the inertial NED frame, where ϕ, θ, and ψ denote roll, pitch, and yaw, respectively, together with the gimbal coordinates $\boldsymbol{a} = [a_1, a_2, a_3, a_4]^T$ associated with the two onboard gyrostabilizers. The corresponding quasi-velocities are collected in the body-fixed vector $\boldsymbol{\nu} = [u, v, w, p, q, r]^T$, while the joint rates are denoted by $\boldsymbol{\omega} = [\omega_1, \omega_2, \omega_3, \omega_4]^T$. Here, ω_1 and ω_3 denote the rotor spin rates of the two gyroscopic units, whereas ω_2 and ω_4 denote the corresponding gimbal precession rates. With these definitions, the kinematic relations assume the standard form

$$\begin{aligned} \dot{\boldsymbol{\eta}} &= \boldsymbol{J}(\boldsymbol{\eta})\,\boldsymbol{\nu}, \\ \dot{\boldsymbol{a}} &= \boldsymbol{\omega}, \end{aligned} \qquad \boldsymbol{J}(\boldsymbol{\eta}) = \begin{bmatrix} \boldsymbol{R}_b^n(\phi,\theta,\psi) & \boldsymbol{0}_{3\times3} \\ \boldsymbol{0}_{3\times3} & \boldsymbol{T}(\phi,\theta) \end{bmatrix}, \tag{1}$$

where $\boldsymbol{R}_b^n(\phi,\theta,\psi)$ is the body-to-NED rotation matrix, constructed according to the roll–pitch–yaw sequence, and $\boldsymbol{T}(\phi,\theta)$ maps the body angular velocity components (p, q, r) into the Euler-angle rates $(\dot{\phi}, \dot{\theta}, \dot{\psi})$.

By introducing the coupled generalized-velocity vector $\boldsymbol{\xi} = \begin{bmatrix} \boldsymbol{\nu} \\ \boldsymbol{\omega} \end{bmatrix} \in \mathbb{R}^{10}$ and the generalized-coordinate vector $\boldsymbol{q} = \begin{bmatrix} \boldsymbol{\eta} \\ \boldsymbol{a} \end{bmatrix}$, the equations of motion can be written in compact form as

$$\begin{aligned} \boldsymbol{M}_{\mathrm{tot}}(\boldsymbol{q})\,\dot{\boldsymbol{\xi}} + \boldsymbol{C}_{\mathrm{tot}}(\boldsymbol{q},\boldsymbol{\xi})\,\boldsymbol{\xi} + \boldsymbol{D}_{\mathrm{tot}}(\boldsymbol{q},\boldsymbol{\xi})\,\boldsymbol{\xi} \\ + \boldsymbol{\tau}_{\mathrm{hs}}(\boldsymbol{q}) + \boldsymbol{\tau}_{\mathrm{mem}}(\boldsymbol{p}) + \boldsymbol{\tau}_g(\boldsymbol{q}) \\ = \boldsymbol{\tau}_{\mathrm{env}}(\boldsymbol{q},\boldsymbol{\xi},t) + \boldsymbol{B}\boldsymbol{u} + \boldsymbol{\tau}_v. \end{aligned} \tag{2}$$

In this formulation, $\boldsymbol{\tau}_{\mathrm{hs}}(\boldsymbol{q})$ denotes the hydrostatic restoring forces and moments, whereas $\boldsymbol{\tau}_{\mathrm{mem}}(\boldsymbol{p})$ accounts for the radiation-memory contribution through an auxiliary linear state-space subsystem with internal states $\boldsymbol{p}$. The term $\boldsymbol{\tau}_g(\boldsymbol{q})$ collects the gravitational actions of the coupled mechanical system. On the right-hand side, $\boldsymbol{\tau}_{\mathrm{env}}(\boldsymbol{q},\boldsymbol{\xi},t)$ includes the external environmental loads, mainly due to waves and wind, while $\boldsymbol{B}\boldsymbol{u}$ represents the control action applied to the gyroscope actuators. Finally, $\boldsymbol{\tau}_v$ denotes the equivalent action required from the steering system to maintain the prescribed heading in the presence of environmental disturbances. In this sense, $\boldsymbol{\tau}_v$ is not intended to reproduce the detailed dynamics of a specific steering actuator, but rather

to provide an equivalent control quantity useful for quantifying the effort demanded from the directional control system.

The overall inertia and Coriolis–centrifugal matrices result from the combination of the rigid-body ship–gyro dynamics and the hydrodynamic added-mass contribution. By partitioning the system according to the hull degrees of freedom and the gyro internal coordinates, one obtains

$$\boldsymbol{M}_{\mathrm{tot}}(\boldsymbol{q}) = \begin{bmatrix} \boldsymbol{M}_{\mathrm{RB}}(\boldsymbol{q}) + \boldsymbol{M}_A & \boldsymbol{M}_{12}(\boldsymbol{q}) \\ \boldsymbol{M}_{12}^{\top}(\boldsymbol{q}) & \boldsymbol{M}_{22} \end{bmatrix}, \qquad \boldsymbol{C}_{\mathrm{tot}}(\boldsymbol{q},\boldsymbol{\xi}) = \begin{bmatrix} \boldsymbol{C}_{\mathrm{RB}}(\boldsymbol{q},\boldsymbol{\nu}) + \boldsymbol{C}_A(\boldsymbol{\nu}) & \boldsymbol{C}_{12}(\boldsymbol{q},\boldsymbol{\xi}) \\ \boldsymbol{C}_{12}^{\top}(\boldsymbol{q},\boldsymbol{\xi}) & \boldsymbol{C}_{22}(\boldsymbol{\omega}) \end{bmatrix}. \tag{3}$$

Here, $\boldsymbol{M}_{\mathrm{RB}}$ denotes the rigid-body inertia matrix of the vessel, including the contribution of the rotor mass offsets, while $\boldsymbol{M}_{22}$ collects the equivalent inertias associated with the gyro joints. The off-diagonal block $\boldsymbol{M}_{12}$ describes the inertial coupling between hull motion and the internal rotating units, and its transpose reflects the underlying Lagrangian structure of the coupled system. In the Coriolis–centrifugal matrix, $\boldsymbol{C}_{\mathrm{RB}}$ and $\boldsymbol{C}_{22}$ represent the rigid-body and internal gyro contributions, respectively, whereas $\boldsymbol{C}_{12}$ accounts for the nonlinear gyroscopic coupling between hull and flywheels. The hydrodynamic terms $\boldsymbol{M}_A$ and $\boldsymbol{C}_A$ are instead associated with added-mass effects and act exclusively on the six hull degrees of freedom.

The hydrodynamic coefficients and hydrostatic parameters were computed with ANSYS AQWA, based on linear potential-flow theory in the frequency domain [16]. The wetted hull was discretized using a boundary-element panel model, and, for each rigid-body degree of freedom, the radiation problem was solved by imposing a unit harmonic velocity in the corresponding direction. This procedure yields the frequency-dependent added-mass and radiation-damping matrices, $\boldsymbol{A}(\omega)$ and $\boldsymbol{B}(\omega)$, together with the hydrostatic restoring coefficients.

Within the time-domain model, the hydrodynamic contribution is introduced in two complementary forms. First, the constant added-mass matrix $\boldsymbol{M}_A \in \mathbb{R}^{6\times 6}$ is taken as the high-frequency limit of $\boldsymbol{A}(\omega)$, consistently with the Cummins formulation [15]. Second, the residual frequency dependence of radiation effects, together with the corresponding memory contribution, is represented through the auxiliary state-space subsystem introduced in the following subsection. In this way, the frequency-domain hydrodynamic data are consistently recast into a time-domain form that contributes both to the added-mass terms and to the internal radiation-memory dynamics.

The hydrodynamic and inertial parameters adopted in the model were further checked against experimental and numerical information made available by Alilauro from previous sea trials and company-led numerical campaigns on vessels of the same class. These data were used as reference information for the main global dynamic properties of the vessel, including the roll natural period, the order of magnitude of the roll damping, and the steady-state response levels observed under representative operating and sea conditions. In particular, the linear roll damping coefficient B_{44} was selected so as to obtain a roll response consistent with the available reference behaviour, while the hydrostatic restoring terms and inertial properties were verified against the vessel loading and stability data. Although this procedure does not constitute a dedicated full-scale validation campaign of the controlled system, it provides an industrial consistency check for the AQWA-based hydrodynamic coefficients and for the time-domain ship model used in the present study.

2.2 Hydrodynamic Memory Term

The representation introduced above is completed by the radiation-memory contribution, which accounts for the frequency dependence of the hydrodynamic forces not captured by the constant added-mass matrix alone. In the frequency domain, this effect is described by the

radiation impedance function $K_{ij}(\mathrm{i}\omega)$, which depends on the added-mass and radiation-damping matrices, $\boldsymbol{A}(\omega)$ and $\boldsymbol{B}(\omega)$, obtained from the AQWA analysis.

To obtain a form suitable for time-domain simulation, each entry of the radiation matrix is approximated by a stable finite-order rational function [15]. Its state-space realization introduces an auxiliary state vector $\boldsymbol{p} \in \mathbb{R}^{n_p}$ governed by

$$\begin{aligned} \dot{\boldsymbol{p}} &= \boldsymbol{A}_r\, \boldsymbol{p} + \boldsymbol{B}_r\, \boldsymbol{\nu}, \\ \boldsymbol{\mu} &= \boldsymbol{C}_r\, \boldsymbol{p}, \end{aligned} \tag{4}$$

where n_p denotes the total order selected for the rational approximation of the radiation terms K_{ij}, while $\boldsymbol{A}_r$, $\boldsymbol{B}_r$, and $\boldsymbol{C}_r$ are the state-space matrices of the resulting finite-order realization of the radiation-memory operator. In particular, $\boldsymbol{A}_r$ governs the internal memory dynamics, $\boldsymbol{B}_r$ maps the hull velocities into the auxiliary states, and $\boldsymbol{C}_r$ reconstructs the corresponding radiation-memory loads. The vector $\boldsymbol{p}$ therefore represents the internal states required to reproduce the frequency-dependent radiation response in the time domain. The corresponding memory load is applied only to the six hull degrees of freedom, namely

$$\boldsymbol{\tau}_{\mathrm{mem}} = \begin{bmatrix} \boldsymbol{\mu} \\ \boldsymbol{0}_{4\times 1} \end{bmatrix}. \tag{5}$$

This construction allows the radiation-memory effects extracted from the frequency-domain hydrodynamic analysis to be embedded into the nonlinear ship–gyro model through a finite-dimensional internal subsystem, while preserving an overall coupled ODE formulation.

2.3 Damping and Restoring Terms

The dissipative effects of the system are modelled by considering jointly the hydrodynamic contributions and those associated with the gyroscopic system. The total damping term is written as

$$\boldsymbol{D}_{\mathrm{tot}}(\boldsymbol{q}, \boldsymbol{\xi}) = \begin{bmatrix} (\boldsymbol{D}_l + \boldsymbol{D}_n(\boldsymbol{\nu}))\, \boldsymbol{\nu} \\ \boldsymbol{Q}_c(\boldsymbol{\omega}) \end{bmatrix} \tag{6}$$

where $\boldsymbol{D}_l$ is the linear hydrodynamic damping matrix, $\boldsymbol{D}_n(\boldsymbol{\nu})$ collects the state-dependent nonlinear dissipative contributions, and $\boldsymbol{Q}_c(\boldsymbol{\omega})$ accounts for the internal dissipation of the gyroscopic system associated with gimbal motion.

The linear term $\boldsymbol{D}_l$ includes both the potential damping contribution, derived from the radiation damping matrices computed with ANSYS AQWA, and a viscous correction introduced to capture dissipative effects not accounted for by potential theory. For the roll degree of freedom in particular, the damping coefficient is assigned by prescribing a target modal damping ratio, following [15]:

$$B_{44} = 2\zeta_{\mathrm{roll}}\, \omega_{\mathrm{roll}}\, (I_x + A_{44}(\omega_{\mathrm{roll}})) \tag{7}$$

The nonlinear contributions $\boldsymbol{D}_n(\boldsymbol{\nu})$ introduce quadratic terms in the manoeuvring velocities following the standard formulation [15].

The hydrostatic restoring contribution is modelled using a linearised metacentric approach about the static equilibrium configuration:

$$\boldsymbol{\tau}_{\mathrm{hs}}(\boldsymbol{q}) = \begin{bmatrix} \boldsymbol{G}(\boldsymbol{\eta} - \boldsymbol{\eta}_0) \\ \boldsymbol{0}_{4\times 1} \end{bmatrix} \tag{8}$$

where $\boldsymbol{G}$ is the hydrostatic stiffness matrix and $\boldsymbol{\eta}_0$ is the equilibrium attitude.

2.4 Environmental disturbances

Wave-induced forces and moments are reconstructed in the time domain starting from the *Response Amplitude Operators* (RAOs) computed with ANSYS AQWA in the frequency domain. In all simulations, a constant forward speed $U = 20$ knots is assumed, consistent with the linear potential flow theory underlying the hydrodynamic model.

The sea state is generated through a spectral discretization of the wave field, parametrized by the wind speed selected according to the Beaufort scale. The spectrum is divided into N harmonic components characterized by frequency ω_i, random phase ϕ_i, and direction β_i, with amplitudes determined by the local spectral energy. For each degree of freedom j, the wave force (or moment) in the time domain is therefore obtained as

$$\tau_{\text{wave},j}(t) = \sum_{i=1}^{N} \left|\text{RAO}_j(U, \omega_i, \beta_i)\right| \sqrt{2S(\omega_i)\,\Delta\omega_i}\, \cos\!\big(\omega_i t + \phi_i + \theta_j(U, \omega_i, \beta_i)\big) \tag{9}$$

where U is the vessel cruising speed, $S(\omega_i)$ is the spectral density evaluated at frequency ω_i, and $\theta_j(U, \omega_i, \beta_i)$ is the phase of the corresponding RAO. The directions β_i are distributed around a mean direction with a prescribed spreading, in order to represent directional sea states.

The wind action $\boldsymbol{\tau}_{\text{wind}}$ is modeled as the combination of a mean component and a gust component, with aerodynamic forces and moments derived from the relative wind velocity using angle-dependent dimensionless coefficients, according to standard formulations [15].

In the overall dynamic model, the environmental loads are finally introduced as

$$\boldsymbol{\tau}_{\text{env}}(\boldsymbol{q}, \boldsymbol{\xi}, t) = \begin{bmatrix} \boldsymbol{\tau}_{\text{wave}}(t, \boldsymbol{\eta}, \boldsymbol{\nu}) + \boldsymbol{\tau}_{\text{wind}}(t, \boldsymbol{\eta}, \boldsymbol{\nu}) \\ \mathbf{0}_{4\times 1} \end{bmatrix} \tag{10}$$

so that they act exclusively on the six degrees of freedom of the hull.

3 CONTROL STRATEGY DESIGN

The control strategy is developed starting from the nonlinear ship–gyro model introduced in the previous section, with the objective of actively shaping the coupled roll–yaw response of the vessel while preserving the operability of the gyrostabilizers within their admissible working range. In the proposed framework, control design is driven by the specification of suitable performance objectives, rather than by the sole stabilization of a prescribed equilibrium. To this end, the Feedback Local Optimality Principle (FLOP) is adopted as the synthesis tool.

FLOP is particularly attractive in the present application for two main reasons. First, it enables the derivation of a feedback control law $\boldsymbol{u}(\boldsymbol{x})$ directly from a nonlinear affine model, making it suitable for strongly coupled ship–gyro dynamics. Second, it allows the desired closed-loop behavior to be encoded through a state-dependent shaping function $\gamma(\boldsymbol{x})$, so that roll attenuation, directional stabilization, comfort-related requirements, and actuator-related soft constraints can all be incorporated within a unified model-based formulation. In this sense, the effectiveness of the controller depends not only on the dynamical model employed for synthesis, but also on the way the shaping function is constructed to reflect the actual performance targets of interest.

3.1 Control-oriented model

The complete nonlinear model described in Section 2 is retained as the reference plant for numerical simulation and performance assessment. Such a model includes the full set of rigid-body, hydrodynamic, hydrostatic, gyroscopic, and environmental contributions required

to reproduce the vessel response under realistic operating conditions. For feedback synthesis, however, a control-oriented representation is adopted. The latter is derived from the full model by retaining only the state variables that are both relevant to the control objectives and reasonably available through onboard measurements or state estimation.

In particular, the control-oriented formulation preserves all the intrinsic dynamic contributions of the vessel–gyroscope system, including the total inertia matrix $\boldsymbol{M}_{\mathrm{tot}}(\boldsymbol{q})$, the Coriolis and centripetal terms $\boldsymbol{C}_{\mathrm{tot}}(\boldsymbol{q},\boldsymbol{\xi})$, the hydrodynamic damping $\boldsymbol{D}_{\mathrm{tot}}(\boldsymbol{q},\boldsymbol{\xi})$, the hydrostatic restoring forces $\boldsymbol{\tau}_{\mathrm{hs}}(\boldsymbol{q})$, the radiation memory effects $\boldsymbol{\tau}_{\mathrm{mem}}(\boldsymbol{p})$, and the gravity contribution $\boldsymbol{\tau}_{g}(\boldsymbol{q})$. All these terms depend exclusively on quantities that are either directly measured or reconstructable from standard onboard instrumentation: the vessel attitudes and angular rates involved in roll–yaw dynamics, available from inertial measurement units, and the gimbal coordinates and angular velocities of both gyrostabilizers, available from actuator encoders. In the comfort-oriented configuration, the vertical acceleration at the passenger reference point P, see Figure 1, is also assumed to be available, either through direct measurement or through onboard state reconstruction. By contrast, the environmental disturbance loads, and the equivalent steering action are not assumed to be directly measurable and are therefore treated as internal dynamics or exogenous inputs acting on the plant, rather than as feedback variables entering the control law explicitly.

Under these assumptions, the control-oriented model is written in the affine nonlinear form

$$\dot{\boldsymbol{x}} = \boldsymbol{\phi}(\boldsymbol{x}) + \boldsymbol{H}\boldsymbol{u}, \tag{11}$$

where $\boldsymbol{x} \in \mathbb{R}^n$ is the control-state vector, $\boldsymbol{u} \in \mathbb{R}^m$ is the actuator input vector, $\boldsymbol{H}$ is the input distribution matrix, and $\boldsymbol{\phi}(\boldsymbol{x})$ collects the uncontrolled nonlinear dynamics retained in the feedback model. This distinction between the high-fidelity plant and the reduced control-oriented model is essential: the former is used to evaluate the actual closed-loop response of the vessel, while the latter provides the structure required for real-time model-based control synthesis.

3.2 FLOP-based feedback synthesis

Within the affine model above, the control law is derived through the Feedback Local Optimality Principle. The method is formulated around an equilibrium pair $(\boldsymbol{x}_T, \boldsymbol{u}_T)$ satisfying

$$\boldsymbol{\phi}(\boldsymbol{x}_T) + \boldsymbol{H}\boldsymbol{u}_T = \boldsymbol{0}, \tag{12}$$

from which the corresponding trim control input is obtained as

$$\boldsymbol{u}_T = -\boldsymbol{H}^{+}\boldsymbol{\phi}(\boldsymbol{x}_T), \tag{13}$$

where $\boldsymbol{H}^{+}$ denotes the pseudo-inverse of $\boldsymbol{H}$.

Introducing the equilibrium-relative variables $\tilde{\boldsymbol{x}} = \boldsymbol{x} - \boldsymbol{x}_T$ and $\tilde{\boldsymbol{u}} = \boldsymbol{u} - \boldsymbol{u}_T$, the performance functional is written as

$$J = \int_0^T \left[\frac{1}{2}\tilde{\boldsymbol{u}}^T \boldsymbol{R}\tilde{\boldsymbol{u}} + \gamma(\tilde{\boldsymbol{x}}) + \boldsymbol{\lambda}^T \left(\dot{\tilde{\boldsymbol{x}}} - \left(\boldsymbol{\phi}(\tilde{\boldsymbol{x}} + \boldsymbol{x}_T) + \boldsymbol{H}(\tilde{\boldsymbol{u}} + \boldsymbol{u}_T) \right) \right) \right] dt, \tag{14}$$

where $\boldsymbol{R}$ is a positive-definite weighting matrix penalizing control effort, $\gamma(\tilde{\boldsymbol{x}})$ is the state-dependent shaping function encoding the desired closed-loop behavior, and $\boldsymbol{\lambda}$ is the Lagrange multiplier associated with the system dynamics.

Applying the variational procedure with respect to $\tilde{\boldsymbol{x}}$, $\tilde{\boldsymbol{u}}$, and $\boldsymbol{\lambda}$, and imposing the augmented FLOP condition

$$\dot{\boldsymbol{\lambda}} = -\frac{1}{\Delta\tau}\boldsymbol{\lambda}, \tag{15}$$

where $\Delta\tau > 0$ is a virtual time parameter and $\boldsymbol{\lambda}(T) = \mathbf{0}$ is the transversality condition, one obtains the feedback law in the original variables as

$$\boldsymbol{u} = \boldsymbol{R}^{-1}\boldsymbol{H}^T \left[\left(\nabla_{\boldsymbol{x}} \boldsymbol{\phi}(\boldsymbol{x})^T - \frac{1}{\Delta\tau}\boldsymbol{I} \right)^{-1} \nabla_{\boldsymbol{x}} \gamma(\boldsymbol{x}) \right] + \boldsymbol{u}_T. \tag{16}$$

An important feature of this formulation is that the control action is computed algebraically from the current state, without the need for online trajectory optimization or the numerical integration of auxiliary adjoint equations. As a result, the computational burden remains limited even when nonlinear shaping terms are introduced through $\gamma(\boldsymbol{x})$, which makes the method particularly attractive for real-time applications in nonlinear marine systems, consistent with previous FLOP-based developments by the authors in related maritime contexts [17].

3.3 Task-oriented shaping function

Within the FLOP framework, the shaping function $\gamma(\boldsymbol{x})$ is the central design element of the controller. Rather than acting as a generic state penalty, it is conceived here as a task-oriented potential that determines which dynamical features of the ship–gyro system are to be promoted or suppressed. Its design therefore reflects the specific objectives of the present study: reduction of roll motion, support to directional stabilization through yaw-related effects, improvement of passenger comfort in a dedicated control configuration, and soft enforcement of actuator limitations.

This interpretation is particularly relevant in the present application, since the same control synthesis procedure can generate different feedback behaviors depending on the structure assigned to $\gamma(\boldsymbol{x})$. In other words, FLOP provides the synthesis mechanism, whereas the actual control objective is encoded by the shaping function. For this reason, the latter is designed so as to explicitly reflect the performance indicators discussed in the introduction, rather than relying on roll attenuation alone as a surrogate for overall performance.

Accordingly, the shaping function is defined as

$$\gamma(\boldsymbol{x}) = w_\phi \phi^2 + w_p p^2 + w_\psi \psi^2 + w_r r^2 + w_s \left(\omega_1^2 + \omega_3^2 \right) + w_a \left(a_{P,z}^{(n)}(\boldsymbol{x}) \right)^2 + \gamma_{\text{bar}}(\boldsymbol{x}), \tag{17}$$

where ϕ and p denote the roll angle and roll rate, respectively, ψ and r are the yaw angle and yaw rate, ω_1 and ω_3 are the spin velocities of the two gyroscopic units, and $a_{P,z}^{(n)}(\boldsymbol{x})$ is the vertical acceleration of the reference point P expressed in the inertial frame. The scalar coefficients w_ϕ, w_p, w_ψ, w_r, w_s, and w_a determine the relative importance assigned to roll reduction, directional stabilization, gyroscope usage, and comfort enhancement.

The term involving $a_{P,z}^{(n)}(\boldsymbol{x})$ is introduced only in the comfort-oriented configuration, and provides a direct proxy for the vertical-acceleration criterion underlying ISO 2631. In this way, the control objective can be explicitly aligned with a metric more closely related to passenger discomfort, instead of being defined solely in terms of angular ship motion. Conversely, in the roll-oriented and asynchronous configurations, the corresponding weight can be reduced or set to zero, so that the shaping function emphasizes roll attenuation and yaw-related performance.

3.4 Soft constraints on gyro operation

In addition to the quadratic performance terms, the shaping function includes a nonlinear barrier contribution used to discourage operation near the precession-speed limits of the gyrostabilizers. This allows actuator-related soft constraints to be incorporated directly into the control objective, without the need for explicit constrained optimization.

Denoting by $\omega_{\max}$ the maximum admissible precession speed, the barrier term is taken as

$$\gamma_{\text{bar}}(\boldsymbol{x}) = -w_{\text{bar}} \left[\log\left(1 - \left(\frac{\omega_2}{\omega_{\max}}\right)^2\right) + \log\left(1 - \left(\frac{\omega_4}{\omega_{\max}}\right)^2\right) \right], \tag{18}$$

where ω_2 and ω_4 are the precession rates of the two gimbals and w_{bar} is a scalar tuning parameter. As the precession speeds approach their admissible bounds, $\gamma_{\text{bar}}(\boldsymbol{x})$ increases sharply, thereby inducing the feedback law to reduce the control action and keeping the system away from mechanically critical configurations.

This feature is especially relevant in the present framework, since the FLOP control law depends directly on the gradient of the shaping function. As a consequence, smooth nonlinear penalties such as $\gamma_{\text{bar}}(\boldsymbol{x})$ can be embedded into the feedback synthesis in a natural way, preserving an entirely algebraic control structure while still accounting for the practical operating limits of the gyrostabilizers.

4 RESULTS AND DISCUSSION

The simulation campaign is designed to cover a representative set of operating conditions for high-speed passenger craft, by combining two sea severities (*Sea State 3* and *Sea State 4*) with two wave headings ($\beta = 90°$ and $\beta = 45°$ with respect to the vessel heading). This choice makes it possible to assess the controller response under both moderate and more demanding environmental excitation, while also examining the effect of wave incidence on the relative contribution of roll and pitch to the overall vessel dynamics and onboard comfort. Each simulation covers a duration of 20 minutes, consistent with the exposure window required by ISO 2631-1 for the evaluation of motion sickness indices.

For each scenario, five configurations are compared: *Uncontrolled*, *Passive*, *FLOP (Roll)*, *FLOP (Comfort)*, and *FLOP (Async)*. These are obtained by selectively activating the weights of the FLOP cost function in Eq. 17: *FLOP (Roll)* activates w_ϕ and w_p only, suppressing yaw, precession velocity, and comfort terms; *FLOP (Comfort)* activates w_a only, directing all control authority towards the minimisation of vertical accelerations; *FLOP (Async)* activates w_ϕ, w_p, w_r, and w_s, enabling simultaneous roll stabilisation and yaw moment generation through asymmetric precession of the two gyroscopes.

The main performance indicators are the roll RMS, the comfort index MDSV_z, the power absorbed by the gyrostabilizers, and the equivalent rudder power required for heading keeping. The comfort index MDSV_z is defined in accordance with ISO 2631-1 [1] as the square root of the time integral of the squared frequency-weighted vertical acceleration at a representative passenger location over the exposure duration:

$$\text{MDSV}_z = \left(\int_0^T a_{w,z}^2(t)\, \mathrm{d}t \right)^{1/2} \tag{19}$$

where $a_{w,z}(t)$ is the vertical acceleration filtered by the ISO 2631-1 frequency weighting W_f, which emphasises the 0.1–0.5 Hz band most associated with motion sickness, and $T = 1200$ s.

Higher values of $MDSV_z$ correspond to greater motion sickness exposure. The acceleration is evaluated at a fixed measurement point P located forward of the centre of gravity (see Figure 1), which represents the most demanding passenger location: due to its longitudinal and lateral offset from the CoM, the vertical acceleration at P receives contributions from both roll and pitch, making it sensitive to the coupled rotational dynamics that the control system is designed to attenuate. The corresponding results are summarised in Tables 3 and 4.

In moderate beam-sea conditions (Sea State 3, $\beta = 90°$), passive stabilization already provides a significant reduction of roll motion, lowering the roll RMS by about 40% with respect to the uncontrolled case. However, the benefit of active feedback is immediately evident: *FLOP (Roll)* increases the reduction to about 68% while requiring nearly the same gyro power, showing that feedback control makes substantially more effective use of the available actuation authority. In the same condition, *FLOP (Comfort)* produces the lowest $MDSV_z$ of the entire campaign, with an 18% reduction with respect to the uncontrolled case and a 12% improvement over *FLOP (Roll)*, although at the expense of a more limited roll reduction. This behavior confirms that the comfort-oriented formulation does not seek roll attenuation per se, but rather acts on the spectral content of the vertical acceleration that is most relevant to passenger discomfort. Under the same beam-sea condition, *FLOP (Async)* preserves a roll reduction comparable to that of *FLOP (Roll)* while reducing the equivalent rudder power by about 14% in both RMS and 95th-percentile terms, with only a marginal increase in gyro power. This result highlights the practical value of exploiting the gyroscopically generated yaw moment as an additional control resource.

When the wave heading is changed to $\beta = 45°$ in Sea State 3, the vertical acceleration field is no longer governed primarily by roll, since pitch becomes a comparably important contributor. In this case, *FLOP (Roll)* still achieves a substantial roll reduction (about 52%) together with a slight improvement in $MDSV_z$. By contrast, *FLOP (Comfort)* becomes essentially ineffective from the standpoint of comfort and strongly penalizing in terms of roll response: the roll RMS almost doubles with respect to the uncontrolled case, while $MDSV_z$ remains practically unchanged. The reason is structural rather than numerical: in oblique-wave conditions, the dominant contribution to the vertical acceleration arises from pitch, which is not directly controllable with the adopted two-gyro architecture. As a consequence, the comfort-oriented controller attempts to optimize a metric whose dominant physical contributors are only weakly influenced by the available control authority, thereby sacrificing roll attenuation without obtaining a meaningful benefit in comfort. In the same condition, *FLOP (Async)* remains close to *FLOP (Roll)* in terms of roll mitigation, but the reduction in rudder effort is much smaller than in beam sea, as expected. The trends become even more evident in Sea State 4, where the increased wave energy brings the gyrostabilizers closer to their admissible operating limits. In beam sea ($\beta = 90°$), the weakness of passive operation becomes clear: the roll reduction is only about 5%, indicating that a passive device alone is unable to adapt its action to the instantaneous nonlinear response of the vessel. Under the same conditions, *FLOP (Roll)* still achieves a 32% reduction of the roll RMS, despite the stronger excitation and the more frequent approach to precession saturation. The comfort-oriented configuration continues to exhibit the same trade-off already observed in Sea State 3: it provides a moderate reduction in $MDSV_z$ (about 7% with respect to the uncontrolled case), but does so by pushing the gyros systematically closer to their operating limits, as indicated by the 95th-percentile gyro power approaching the nominal installed limit. Once again, *FLOP (Async)* yields a system-level advantage by reducing the equivalent rudder power by about 5% in RMS and 8% in 95th-percentile terms relative to *FLOP (Roll)*, while preserving a comparable level of roll attenuation.

The most severe condition of the whole campaign corresponds to Sea State 4 with $\beta = 45°$,

Table 3: Main performance metrics in Sea State 3.

β	Configuration	Roll RMS [deg]	MDSV$_z$ [$m\ s^{-1.5}$]	P_{Gyro} [kW]	$P_{\text{Gyro,95}}$ [kW]	P_{Rudder} [kW]	$P_{\text{Rudder,95}}$ [kW]
90°	Uncontrolled	0.603	3.869	0.000	0.000	10.733	23.367
90°	Passive	0.361	3.609	4.852	8.811	10.236	22.686
90°	FLOP (Roll)	0.192	3.633	5.142	9.364	10.460	23.316
90°	FLOP (Comfort)	0.466	3.187	5.885	10.504	10.535	23.368
90°	FLOP (Async)	0.197	3.660	5.473	10.082	8.963	20.150
45°	Uncontrolled	0.160	3.223	0.000	0.000	2.455	5.451
45°	Passive	0.083	3.106	3.760	6.953	2.178	4.765
45°	FLOP (Roll)	0.077	3.092	4.468	8.208	2.317	5.151
45°	FLOP (Comfort)	0.306	3.213	7.614	14.403	2.316	5.170
45°	FLOP (Async)	0.090	3.084	4.929	8.851	2.296	5.084

where the uncontrolled MDSV$_z$ exceeds 22. In this case, *FLOP (Roll)* provides both the largest roll reduction among the tested strategies (about 59%) and the best comfort performance among the controlled configurations. *FLOP (Comfort)* again proves detrimental: MDSV$_z$ becomes slightly worse than in the roll-oriented case, while the gyro RMS power increases by about 23%. This confirms that the comfort-oriented shaping function is effective only when the controlled degrees of freedom are also the dominant contributors to the comfort metric. The asynchronous strategy, on the other hand, maintains a roll response very close to that of *FLOP (Roll)* and still provides a modest reduction in rudder effort, although the benefit is less pronounced than in beam sea because the coupling between gyro-generated yaw moments and steering demand is intrinsically weaker in oblique-wave conditions.

Taken together, these results show that no single strategy is uniformly optimal over the entire operating envelope. *FLOP (Roll)* is the most robust solution, consistently delivering the best compromise between roll attenuation and actuator usage. *FLOP (Comfort)* is beneficial only when roll is the dominant source of the vertical accelerations perceived onboard, and therefore should be activated only under conditions in which the comfort metric is genuinely aligned with the controllable dynamics of the two-gyro system. *FLOP (Async)*, instead, is the most attractive option when the stabilization problem is interpreted at the system level, since it enables a redistribution of control authority between roll mitigation and yaw management, yielding a tangible reduction of steering effort with only a limited increase in gyro power.

5 Conclusions

This work assessed the effectiveness of a pair of onboard gyrostabilizers for roll mitigation in a high-speed passenger catamaran under irregular-sea conditions, by comparing passive operation with different FLOP-based active control strategies. The results show that the use of feedback is essential to exploit the available gyro authority effectively: while the *Passive* configuration provides limited benefits, especially in severe seas, the FLOP-controlled cases achieve significantly larger roll reduction by driving the gyros close to their admissible precession limits in a controlled and purposeful way.

Among the tested strategies, *FLOP (Roll)* proved to be the most robust solution over the considered operating conditions, consistently providing the best compromise in terms of roll attenuation and actuator usage. *FLOP (Comfort)* was shown to be beneficial only when roll is

Table 4: Main performance metrics in Sea State 4.

β	Configuration	Roll RMS [deg]	MDSV$_z$ [$m\ s^{-1.5}$]	P_{Gyro} [kW]	$P_{\text{Gyro,95}}$ [kW]	P_{Rudder} [kW]	$P_{\text{Rudder,95}}$ [kW]
90°	Uncontrolled	2.298	14.462	0.000	0.000	40.283	92.097
90°	Passive	2.180	14.096	14.001	26.108	37.728	86.146
90°	FLOP (Roll)	1.557	14.856	14.262	30.411	38.013	87.899
90°	FLOP (Comfort)	2.243	13.426	17.380	35.197	37.080	83.812
90°	FLOP (Async)	1.749	14.774	14.563	29.490	35.984	80.790
45°	Uncontrolled	1.323	22.062	0.000	0.000	11.592	25.401
45°	Passive	0.686	21.010	9.343	17.320	11.727	25.532
45°	FLOP (Roll)	0.548	20.829	9.638	17.639	12.526	27.601
45°	FLOP (Comfort)	0.885	21.312	11.891	21.790	11.839	25.732
45°	FLOP (Async)	0.571	20.850	9.669	17.861	11.576	25.285

the dominant contributor to the comfort metric, whereas it becomes ineffective, and in some cases detrimental, when pitch-driven vertical accelerations prevail. This highlights a structural limitation of the adopted two-gyro configuration, which has direct control authority mainly on roll and yaw. *FLOP (Async)* provided an additional system-level benefit by exploiting the yaw moment generated by the gyros to reduce rudder effort, particularly in beam-sea conditions, while maintaining roll mitigation comparable to the synchronous roll-oriented strategy.

From an operational standpoint, the rudder-power reduction achieved by *FLOP (Async)* (up to 14% in the investigated beam-sea conditions) indicates a lower equivalent steering demand, with potential benefits in terms of actuator loading, thermal duty, and long-term wear in high-frequency passenger service. The comfort-oriented gains in MDSV$_z$ observed under roll-dominated sea states are also relevant for practical operation, since passenger discomfort and motion-sickness risk can influence route availability, service quality, and the operability limits adopted by operators. Importantly, the proposed strategies act at the level of the feedback law and exploit the existing gyrostabilizer actuation mechanism, without requiring a change in the basic two-gyro layout. This suggests that, after appropriate real-time implementation, sensor integration, and tuning, the active strategy could be selected according to the prevailing sea state and route-specific priorities, such as roll attenuation, comfort improvement, or steering-load reduction.

Overall, the results indicate that gyrostabilizer performance depends not only on actuator size, but also on the choice of control objective and on the interaction between wave direction, sea severity, and controlled degrees of freedom. Future work will investigate the inclination of the gyro precession axis in order to extend the control action to pitch-related motions and thus improve comfort-oriented performance also in oblique-wave conditions. In addition, the proposed FLOP approach will be compared with predictive control strategies, in order to further assess the trade-off between constraint handling, computational demand, and achievable closed-loop performance.

6 ACKNOWLEDGEMENTS

The authors received financial support for the research activities within the project “AIRONE 5.0 – Hybrid vessel for high-speed maritime transport” (Project Number F/350062/01-03/X60), funded under the Innovation Agreement DM 31-12-2021 by the Italian Ministry of Enterprises

and Made in Italy.

REFERENCES

[1] International Organization for Standardization. *Mechanical vibration and shock — Evaluation of human exposure to whole-body vibration — Part 1: General requirements*. ISO 2631-1:1997. Geneva, Switzerland: International Organization for Standardization, 1997.

[2] Tristan Perez and Mogens Blanke. "Ship Roll Damping Control". In: *Annual Reviews in Control* 36.1 (2012), pp. 129–147. DOI: 10.1016/j.arcontrol.2012.03.010.

[3] Tristan Perez and Peter Steinmann. "Analysis of Ship Roll Gyrostabiliser Control". In: *Proceedings of the 8th IFAC International Conference on Manoeuvring and Control of Marine Craft (MCMC 2009)*. Vol. 42. IFAC Proceedings Volumes 18. Guarujá, Brazil, 2009, pp. 310–315. DOI: 10.3182/20090916-3-BR-3001.0060.

[4] Nicholas C. Townsend and R. Ajit Shenoi. "Control Strategies for Marine Gyrostabilizers". In: *Ocean Engineering* 41 (2012), pp. 100–111. DOI: 10.1016/j.oceaneng.2011.12.019.

[5] Murugan Palraj and Palanivel Rajamanickam. "Motion Control of a Barge Ship Using Gyrostabilizer". In: *Ocean Engineering* 209 (2021), p. 107500. DOI: 10.1016/j.oceaneng.2020.107500.

[6] Alejandro Donaire and Tristan Perez. "Energy-Based Nonlinear Control of Ship Roll Gyro-Stabiliser with Precession Angle Constraints". In: *Proceedings of the 9th IFAC Conference on Control Applications in Marine Systems (CAMS 2013)*. Vol. 46. IFAC Proceedings Volumes 33. Osaka, Japan, 2013, pp. 328–333. DOI: 10.3182/20130918-4-JP-3022.00059.

[7] Tristan Perez and Peter Steinmann. "Gyro-Stabilised High-Speed Trimarans". In: *Proceedings of the RINA International Conference on Innovation in High Speed Marine Vessels*. Fremantle, Australia, 2009.

[8] Hiroshi Kurokawa. "Survey of Theory and Steering Laws of Single-Gimbal Control Moment Gyros". In: *Journal of Guidance, Control, and Dynamics* 30.5 (2007), pp. 1331–1340. DOI: 10.2514/1.27316.

[9] Frederick A. Leve, Brian J. Hamilton, and Mason A. Peck. *Spacecraft Momentum Control Systems*. Cham, Switzerland: Springer, 2015. DOI: 10.1007/978-3-319-22563-0.

[10] D. Spitaleri et al. "Enhancing Spherical Rolling Robot Control for Slippery Terrain". In: *13th International Workshop on Robot Motion and Control, RoMoCo 2024 - Proceedings*. 2024, pp. 243–248. DOI: 10.1109/RoMoCo60539.2024.10604310.

[11] Yue Zhang et al. "Real-Time Control of Ship's Roll Motion with Gyrostabilisers". In: *Ocean Engineering* 288 (2023), p. 115946. DOI: 10.1016/j.oceaneng.2023.115946.

[12] Gianluca Pepe et al. "Nonlinear Model-Based Control of a Gyroscopic Stabilization System for High-Speed Crafts". In: *Progress in Marine Science and Technology*. Vol. 10. 2025, pp. 29–36. DOI: 10.3233/PMST250006.

[13] Maicol Laurenza et al. "Adaptive Rendezvous Planning Algorithm for Energy-Efficient Marine Operations". In: *Progress in Marine Science and Technology*. Vol. 10. All Open Access, Hybrid Gold Open Access. 2025, pp. 775–782. DOI: 10.3233/PMST250092.

[14] Maicol Laurenza et al. “Toward Scalable Energy-Efficient Rendezvous Optimization for Multiagent Marine Applications”. In: *IEEE Journal of Oceanic Engineering* (2026). DOI: 10.1109/JOE.2026.3655631.

[15] Thor Fossen. *Handbook of Marine Craft Hydrodynamics and Motion Control*. Apr. 2021. ISBN: 978-1119575047. DOI: 10.1002/9781119994138.

[16] John Nicholas Newman. *Marine Hydrodynamics*. Cambridge, MA: MIT Press, 1977.

[17] Maicol Laurenza et al. “Surface Unmanned Multipurpose Research Marine Vehicle: SUNMARE Project”. In: *Progress in Marine Science and Technology*. Vol. 6. All Open Access, Bronze Open Access, Green Open Access. 2022, pp. 522–529. DOI: 10.3233/PMST220062.